THE JOURNAL OF BIOLOGICAL CHEMISTRY VOL. 288, NO. 20, pp. 14320–14331, May 17, 2013
Published in the U.S.A.

COL6A3 Protein Deficiency in Mice Leads to Muscle and Tendon Defects Similar to Human Collagen VI Congenital Muscular Dystrophy*

Received for publication, November 1, 2012, and in revised form, March 1, 2013 Published, JBC Papers in Press, April 5, 2013, DOI 10.1074/jbc.M112.433078

Te-Cheng Pan[‡], Rui-Zhu Zhang[‡], Dessislava Markova[‡], Machiko Arita[‡], Yejia Zhang[§], Sasha Bogdanovich[¶], Tejvir S. Khurana[¶], Carsten G. Bönnemann[‖], David E. Birk[**], and Mon-Li Chu[‡1]

*From the [‡]Department of Dermatology and Cutaneous Biology, Thomas Jefferson University, Philadelphia, Pennsylvania 19107, [§]Departments of Orthopedic Surgery and Physical Medicine and Rehabilitation, Rush University Medical Center, Chicago, Illinois 60612, [¶]Department of Physiology and Pennsylvania Muscle Institute, University of Pennsylvania School of Medicine, Philadelphia, Pennsylvania 19104, [‖]Neurogenetics Branch, NINDS, National Institutes of Health, Bethesda, Maryland 20824, and **Department of Molecular Pharmacology and Physiology, Morsani College of Medicine, University of South Florida, Tampa, Florida 33612*

Background: The collagen VI COL6A3 subunit may serve critical biological functions independent of the COL6A1 and COL6A2 subunits.
Results: A *Col6a3* mouse mutant displays muscle and tendon abnormalities resembling the *Col6a1*-null mouse.
Conclusion: The primary role of the COL6A3 subunit is in assembling collagen VI microfibrils.
Significance: The *Col6a3* mutant mouse represents an animal model for collagen VI disorders.

Collagen VI is a ubiquitously expressed extracellular microfibrillar protein. Its most common molecular form is composed of the α1(VI), α2(VI), and α3(VI) collagen α chains encoded by the *COL6A1*, *COL6A2*, and *COL6A3* genes, respectively. Mutations in any of the three collagen VI genes cause congenital muscular dystrophy types Bethlem and Ullrich as well as intermediate phenotypes characterized by muscle weakness and connective tissue abnormalities. The α3(VI) collagen α chain has much larger N- and C-globular domains than the other two chains. Its most C-terminal domain can be cleaved off after assembly into microfibrils, and the cleavage product has been implicated in tumor angiogenesis and progression. Here we characterize a *Col6a3* mutant mouse that expresses a very low level of a nonfunctional α3(VI) collagen chain. The mutant mice are deficient in extracellular collagen VI microfibrils and exhibit myopathic features, including decreased muscle mass and contractile force. Ultrastructurally abnormal collagen fibrils were observed in tendon, but not cornea, of the mutant mice, indicating a distinct tissue-specific effect of collagen VI on collagen I fibrillogenesis. Overall, the mice lacking normal α3(VI) collagen chains displayed mild musculoskeletal phenotypes similar to mice deficient in the α1(VI) collagen α chain, suggesting that the cleavage product of the α3(VI) collagen does not elicit essential functions in normal growth and development. The *Col6a3* mouse mutant lacking functional α3(VI) collagen chains thus serves as an animal model for *COL6A3*-related muscular dystrophy.

Collagen VI is a ubiquitously expressed extracellular matrix protein. Its major molecular form is composed of the α1(VI), α2(VI), and α3(VI) α chains, and these collagen VI molecules are assembled into microfibrils. The three α chains each contain a central triple-helical domain of 335–336 amino acids flanked by N- and C-globular domains that are primarily made up of ~200-amino acid modules homologous to the von Willebrand factor type A (VWA)[2] domains (1–3). The α1(VI) and α2(VI) collagen chains are similar in size (140 kDa), having one VWA module in the N-globular domain and two such modules in the C-globular region. The α3(VI) collagen chain is 3 times their size due to substantially larger N- and C-globular domains. Its N-globular domain consists of up to 10 VWA modules, and the C-globular domain contains two VWA and three other protein modules (3, 4). The three α chains fold together into a triple-helical collagen VI molecule (monomer) that further assembles into dimers and tetramers (1, 5). The tetramers are secreted into the extracellular space where they assemble end to end into collagen VI microfibrils (5). Several lines of evidence suggest that the C-terminal end of the α3(VI) collagen chain is cleaved off after microfibrillar assembly (6–8). The cleaved C-terminal domain may serve functions independent of collagen VI microfibrils. For instance, the C-terminal C5 domain of the α3(VI) collagen has been shown to interact with tumor endothelial marker 8 and thereby may play a role in tumor angiogenesis (9). Very recently, the C-terminal cleavage product of the α3(VI) collagen, newly named as "endotrophin," has been shown to promote malignant tumor progression in mice (10).

Additional α3(VI)-like collagen chains, two in humans and three in other animal species, have been identified (11, 12). Current evidence suggests that these α3(VI)-like chains, named

* This work was supported, in whole or in part, by National Institutes of Health Grants AR053251 (to M. L. C.) and AR44745 (to D. E. B.).

[1] To whom correspondence should be addressed: Dept. of Dermatology and Cutaneous Biology, Thomas Jefferson University, 233 S. 10th St., Philadelphia, PA 19107. Tel.: 215-503-4834; Fax: 215-503-5788; E-mail: mon-li.chu@jefferson.edu.

[2] The abbreviations used are: VWA, von Willebrand factor type A; EDL, extensor digitorum longus; ECC, eccentric contraction; ER, endoplasmic reticulum; Xbp-1, X-box-binding protein 1; Bip, chaperone-binding protein; Chop, CCAAT/enhancer-binding protein homologous protein; Hprt1, hypoxanthine phosphoribosyltransferase 1.

α4(VI), α5(VI), and α6(VI) collagens, can replace the α3(VI) collagen and assemble with the α1(VI) and α2(VI) α chains into collagen VI triple-helical monomers (11, 12). However, these α3(VI) collagen-like chains have rather restricted tissue distribution patterns unlike the three major collagen VI chains (13). The effects of the α3(VI)-like chains on collagen VI supramolecular structures remain unclear.

Mutations of the *COL6A1*, *COL6A2*, and *COL6A3* genes encoding the α1(VI), α2(VI), and α3(VI) collagen chains underlie Bethlem myopathy, Ullrich congenital muscular dystrophy, and phenotypes intermediate between Ullrich congenital muscular dystrophy and Bethlem myopathy (14, 15). The signature features of collagen VI-related muscle disorders are early onset muscle weakness in conjunction with connective tissue abnormalities. Ullrich congenital muscular dystrophy is a severe disease characterized by significant muscle weakness, joint contractures, and distal joint hypermobility resembling the Ehlers-Danlos syndrome. Independent ambulation may never be achieved or may be achieved but lost during the first two decades of life due to progressive muscle weakness and joint contractures. Bethlem myopathy is characterized by mild to moderate muscle weakness and multiple progressive joint contractures, mainly affecting the fingers, wrists, elbows, and ankles. It is a slowly progressive disorder and about a half of the Bethlem myopathy patients need aids for mobility after age 50 years (16).

Genotype-phenotype correlations of collagen VI-related muscle disorders are emerging but still incompletely understood. Notably, Allamand *et al.* (14) recently reported that most of the over 200 collagen VI mutations detected to date are distributed in the *COL6A1* and *COL6A2* genes. The finding seems to imply that the α3(VI) collagen α chain, because of its extended N- and C-globular domains, may serve an indispensable function that is distinct from assembling collagen VI microfibrils and to suggest possible phenotypic differences associated with some mutations in *COL6A3.* To investigate whether the phenotype resulting from deficiency of the α3(VI) collagen differs from that of the other two subunits, we set out to generate a mouse mutant with the *Col6a3* gene ablated by gene targeting. However, due to aberrant splicing and insertion of a neomycin gene, the targeted allele transcribed a low level of mutant *Col6a3* mRNA that produced a non-functional protein. We show that the homozygous mutant mice display myopathic and connective tissue symptoms similar to the *Col6a1*-null mice and patients with collagen VI muscle disorders. The results indicate that assembly of collagen VI microfibrils is the main function of the *COL6A3* gene.

EXPERIMENTAL PROCEDURES

Construction of the Targeting Vector—A cosmid clone containing the mouse *Col6a3* gene was isolated from a 129/Sv genomic library by screening with a mouse *Col6a3* cDNA clone (17). A gene-targeting vector was prepared by replacing a 0.65-kb HindIII fragment spanning from exon 15 to intron 16 with a neomycin resistance gene driven by the phosphoglycerol kinase promoter (*Pgk-Neo*) (see Fig. 1*A*). The *Pgk-Neo* gene was inserted in the opposite transcription orientation of the *Col6a3* gene. The targeting vector consisted of a 5.4-kb HindIII fragment as a long arm, a 2.5-kb HindIII fragment as a short arm, and a diphtheria toxin A gene for negative selection.

Generation of the Col6a3 Mutant Mouse—The targeting vector was linearized with NotI and electroporated into mouse 129/Sv embryonic stem (ES) cells. Cells were selected with 250 μg/ml G418. Correctly targeted ES clones were identified by Southern blotting using a DNA probe located externally to the targeted region (see Fig. 1*A*). Targeted clones were injected into C57BL/6 blastocysts and implanted into pseudopregnant females to obtain chimeric mice. The chimeric founders were mated with C57BL/6 mice to generate heterozygous mice, which were then intercrossed to produce wild type, heterozygous, and homozygous mice. Initial phenotype analyses were performed with littermates on a mixed 129/Sv and C57BL/6 background. Mice were backcrossed onto the C57BL/6 background for eight generations and used for further analysis. All animal procedures were performed in accordance with the National Institutes of Health Guidelines for the Care and Use of Laboratory Animals, and all experimental protocols were approved by the Institutional Animal Care and Use Committee of Thomas Jefferson University.

Genotyping of ES Cells and Mice—Genomic DNA isolated from ES cells or mouse tails was digested with BglI, and Southern blot hybridization was performed using a 0.7-kb [^{32}P]dCTP-labeled external probe (see Fig. 1*A*). The probe was generated by PCR amplification of the genomic clone using primers GAGAGGAGATGTCGGGATTCG and GTGAGGCAGCAATGATGTAGAG. Genotyping of the mice was also carried out by PCR amplification of mouse tail DNA. A 521-bp PCR product from the wild type allele was detected using forward primer GCTGACCAATATCCCTCGTG and reverse primer CCAGACAGGCTACAAACTCCA. A product of ~200 bp was amplified from the mutant allele with the same reverse primer and primer GCCAGAGGCCACTTGTGTAG located in the *Pgk-Neo* gene.

Dermal Fibroblasts, Northern Blot, Western Blot, RT-PCR, and Collagen VI Deposition—Dermal fibroblasts were prepared from skin of 3–5-day-old littermates obtained from intercrossing heterozygous animals. Cells were cultured in Dulbecco's modified Eagle's medium (DMEM) with 10% fetal bovine serum (Invitrogen). Northern blotting was performed with total RNA extracted from cells using the RNeasy Mini kit (Qiagen, Valencia, CA) and hybridized with [^{32}P]dCTP-labeled mouse *Col6a1*, *Col6a2*, and *Col6a3* cDNA probes by the procedure described previously (18). RT-PCR analysis of the *Col6a3* mRNA surrounding the gene-targeted region was performed with total RNA isolated from fibroblasts using forward primer TCTTGAACGTGTGGCTAACC and reverse primer CTTTTCTCCAGAAGAACCAGG. For the analysis of collagen VI deposition, fibroblasts were grown in DMEM with 10% FBS in the presence of 50 mg/ml ascorbate phosphate until 5 days after confluence, fixed with 3.7% formaldehyde, and incubated with polyclonal antibodies against α1(VI) or α3(VI) collagens (19, 20) for 1 h. Immunostaining was detected with Cy3-conjugated goat anti-rabbit IgG (1:1000 dilution; Jackson ImmunoResearch Laboratories, West Grove, PA) and observed using a Zeiss Axioskop epifluorescence microscope with a Toshiba

TABLE 1
Real time PCR primer sequences

	Forward primer (5′–3′)	Reverse primer (5′–3′)	Product size
			bp
Hprt1	GAGGAGTCCTGTTGATGTTGCCAG	GAGGAGTCCTGTTGATGTTGCCAG	173
Xbp-1	ACACGCTTGGGAATGGACAC	CCATGGGAAGATGTTCTGGG	170, 144 (spliced)
Bip	AGTTCCCCAGATTGAAGTCAC	CAGGCGGTTTTGGTCATTG	121
Chop	CCCAGGAAACGAAGAGGAAG	GAACTCTGACTGGAATCTGGAG	141
Il-1β	TGGGCTGGACTGTTTCTAATG	TTTCTTGTGACCCTGAGCG	132
Il-6	GAGGATACCACTCCCAACAGACC	AAGTGCATCATCGTTGTTCATACA	140
Tnf-α	CTACCTTGTTGCCTCCTCTTT	GAGCAGAGGTTCAGTGATGTAG	116
Casp-3	TTCATCCAGTCCCTTTGCAG	GGATCTGTTTCTTTGCGTGG	145
Casp-9	AAATCTCCATACCACTGCCTC	TCTTACCCCGATACCCTAACC	115
Bcl-2	GTAAAACCCTCCATCCTGTCC	CCTTTCCTAGACCCAGCAATG	135

3CCD camera and ImagePro software (Media Cybernetics, Silver Spring, MD).

RT-PCR Analysis of Markers for ER Stress, Inflammation, and Apoptosis—Total RNA was isolated from quadriceps muscles and dermal fibroblasts using the RNeasy Mini kit (Qiagen). Muscle tissues were dissected from *Col6a*$^{hm/hm}$ and *Col6a3*$^{+/+}$ littermates at three different ages (5 days, 1 month, and 3 months). Dermal fibroblasts were established from three newborn litters of the *Col6a*$^{hm/hm}$ and *Col6a3*$^{+/+}$ mice. The RNA preparation was treated with DNase I to remove any contaminating genomic DNA. Single-stranded cDNA was synthesized from 0.5 μg of total RNA using RNA to cDNA EcoDry Premix (Clontech) at 42 °C for 1 h. Quantitative real time RT-PCR was performed using SYBR Green PCR Master Mix (Invitrogen/Applied Biosystems (ABI)) on an ABI StepOne Real-Time PCR system. The reaction was initiated at 95 °C for 10 min (to activate the AmpliTaq polymerase) followed by a 40-cycle amplification phase (denaturation at 95 °C for 15 s and annealing/extension at 60 °C for 60 s). A melting curve analysis was performed for each gene to ensure a single PCR product was being amplified with no primer-dimer formation. The amount of PCR product was estimated using a relative standard curve quantification method. The mRNA expression levels of target genes were normalized by hypoxanthine phosphoribosyltransferase 1 (*Hprt1*) mRNA. All the primers used were synthesized by Integrated DNA Technologies, Inc. (Coralville, IA). Statistical analysis was performed using Sigma Plot 11.2 statistical software (Systat Software, Inc.). Primer sequences are shown in Table 1.

Histology and Immunostaining of Tissues—Muscles were dissected, mounted on 10% gum tragacanth, and frozen in liquid nitrogen-cooled isopentane. Sections of 8 μm thick were stained with hematoxylin-eosin. Single fiber areas and the percentage of fibers with central nuclei were determined from images of four different gastrocnemius muscles per group. Approximately 100 fibers from each image taken at 20× magnification were outlined and measured using ImageJ software. For immunostaining, 6–8-μm cryosections were fixed in methanol and incubated with the primary antibodies for 2 h at room temperature. The primary antibodies used were polyclonal antibodies specific for the α1(VI) collagen (20), α3(VI) collagen (19), decorin (LF-113; from Dr. Larry Fisher), tenascin-X (M11; from Dr. Ken-Ichi Matsumoto), NG2 (from Dr. William Stallcup), integrin α7B (U31+; from Dr. Ulrike Mayer), matrilin-2 and -4 (from Dr. Mats Paulsson), and type I collagen (Fitzgerald Industries International, Acton, MA) and a monoclonal antibody for laminin γ1 (Chemicon MAB1914). Cy3-conjugated anti-rabbit or anti-rat IgG (1:800 dilution; Jackson ImmunoResearch Laboratories) was used as the secondary antibody. Nuclei were counterstained with 4′,6′-diamidino-2-phenylindole hydrochloride (DAPI). Fluorescence intensity of the images was measured with ImageJ software.

Physiological Measurements—Ex vivo physiological measurements were performed on dissected extensor digitorum longus (EDL) muscle from 4-month-old male mice as described (21, 22). Muscles were dissected, weighed, and then placed in a custom-built organ bath in oxygenated Ringer's solution (pH 7.4) at 24 °C for the duration of the experiment. The muscle was attached using 5-0 nylon to a Grass FT03 force transducer (Astro-Med, West Warwick, RI) at one end and length controller (precision, 2.5 μm) containing a 1.8° step motor-driven micrometer at the other end. The muscle was stimulated at 25 V using a Grass S48 stimulator to develop an electrical field between two platinum electrodes. Muscle length was adjusted to achieve maximal twitch and tetanic response, and optimal length (Lo) was measured. Muscles were subject to a series of three twitches and three tetanic contractions as well as five eccentric contractions (ECCs) for mechanical property evaluation. Muscles were stimulated using a supramaximal stimulus of 700 ms (500-ms isometric phase and 200-ms eccentric phase) with total lengthening of Lo/10 at the lengthening velocity of 0.5Lo/s. The time between two ECCs was 5 min. ECC force drop was calculated by using the difference of isometric phase of the first and fifth ECCs. Data were digitized and acquired by using a PowerLab/8SP A/D converter and software (AD Instruments, Colorado Springs, CO). Cross-sectional area was determined using the Brooks-Faulkner approximation (23).

Transmission Electron Microscopy—Flexor digitorum longus tendons and corneas were dissected from postnatal day 30 homozygous mutant mice and wild type littermates. Transmission electron microscopy was performed as described previously (24, 25).

Statistical Analysis—Data were analyzed using a paired Student's *t* test and one-way analysis of variance. $p < 0.05$ is considered statistically significant. All data are expressed as mean ± S.E. unless otherwise noted.

RESULTS

Generation of the Col6a3 Mouse Mutant—A gene-targeting vector was designed to disrupt the *Col6a3* gene by replacing the genomic region between the HindIII sites in exon 15 and intron 16 with the *Pgk-Neo* cassette (Fig. 1*A*). Exon 15 encodes a cysteine-rich linker region and the beginning of the triple-helical

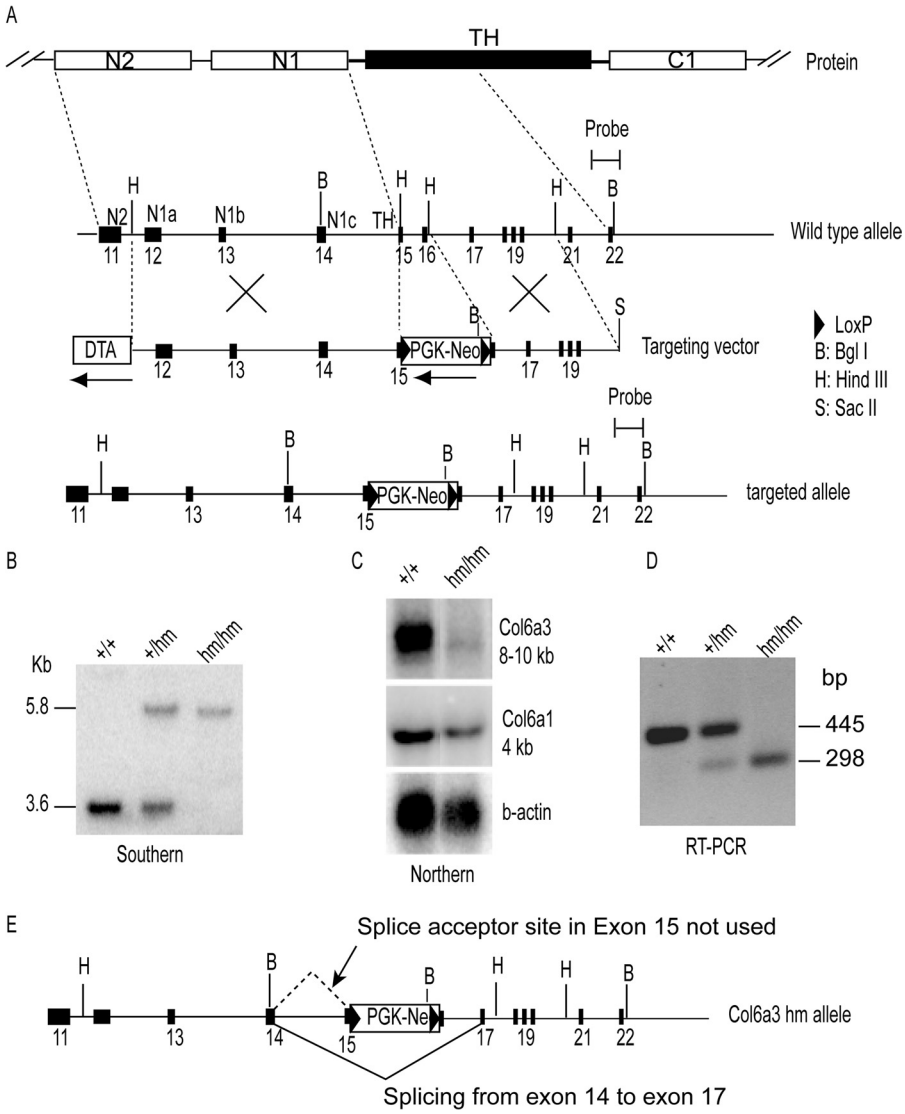

FIGURE 1. **Generation of the *Col6a3* mutant mouse.** *A*, gene targeting of *Col6a3*. The targeting vector contains a 5.4-kb HindIII (*H*) fragment as a long arm, a 2.5-kb HindIII fragment as the short arm, and a *Pgk-Neo* gene flanked by LoxP sequences replacing a HindIII fragment spanning from exon 15 to intron 16 of the *Col6a3* gene. The targeted region encodes two VWA modules in the N-globular domain (*N1* and *N2*) and the N-terminal half of the triple-helical domain (*TH*) of the Col6a3 protein. Restriction sites shown are BglI (*B*), HindIII (*H*), and SacII (*S*). The probe used for Southern blotting is indicated. *B*, Southern blot analysis of mouse tail DNA isolated from *Col6a3*$^{+/+}$, *Col6a3*$^{+/hm}$, and *Col6a3*$^{hm/hm}$ mice. DNA samples were digested with BglI. *C*, Northern blot analysis of total RNA isolated from embryonic fibroblasts of the *Col6a3*$^{+/+}$ and *Col6a3*$^{hm/hm}$ mice using mouse *Col6a3*, *Col6a1*, and β-actin cDNAs as probes. *D*, RT-PCR analysis of total RNA from *Col6a3*$^{+/+}$, *Col6a3*$^{+/hm}$, and *Col6a3*$^{hm/hm}$ mice using primers in exons 14 and 17. *E*, aberrant splicing of the targeted allele. The splice acceptor site in exon 15 of the targeted allele was not used, resulting in skipping of exons 15 and 16 in the mutant mRNA.

domain. Insertion of the *Pgk-Neo* cassette within exon 15 was predicted to yield a premature translational termination codon after the N-globular domain-coding region. Electroporation of the construct into mouse ES cells resulted in ~350 neomycin-resistant clones of which eight were correctly targeted clones based on Southern blot analysis. Three of the positive clones were injected into mouse blastocysts, and 14 chimeric mice were obtained. The targeted allele was transmitted through the germ line to the next generation, and intercrossing of the heterozygous F1 mice from each ES cell clone generated offspring of the three genotypes at the expected Mendelian frequencies (Fig. 1*B*). The homozygous *Col6a3* mutant mice developed normally, were fertile, and did not show overt phenotypic abnormalities. They have normal life spans and have survived beyond 2 years of age.

Unexpectedly, Northern blot analysis revealed that the homozygous mutant synthesized a very low level of a slightly smaller α3(VI) collagen mRNA (Fig. 1*C*). RT-PCR analysis using primers flanking the gene-targeted region confirmed that the α3(VI) collagen mRNA produced by the homozygous mouse was indeed smaller than the normal *Col6a3* mRNA (Fig. 1*D*). Analysis of the heterozygous mouse showed that the mutant transcript was present at a substantially lower level compared with the normal *Col6a3* mRNA (Fig. 1*D*). Quantitative RT-PCR analysis indicated that the mutant mRNA was expressed at a level ~5% of the wild type mRNA (data not shown). DNA sequencing identified an in-frame deletion of 147 bp in the mutant mRNA that corresponded to the sequences encoded by exons 15 and 16. The results indicated that the splice acceptor site in exon 15 was not utilized and thereby led

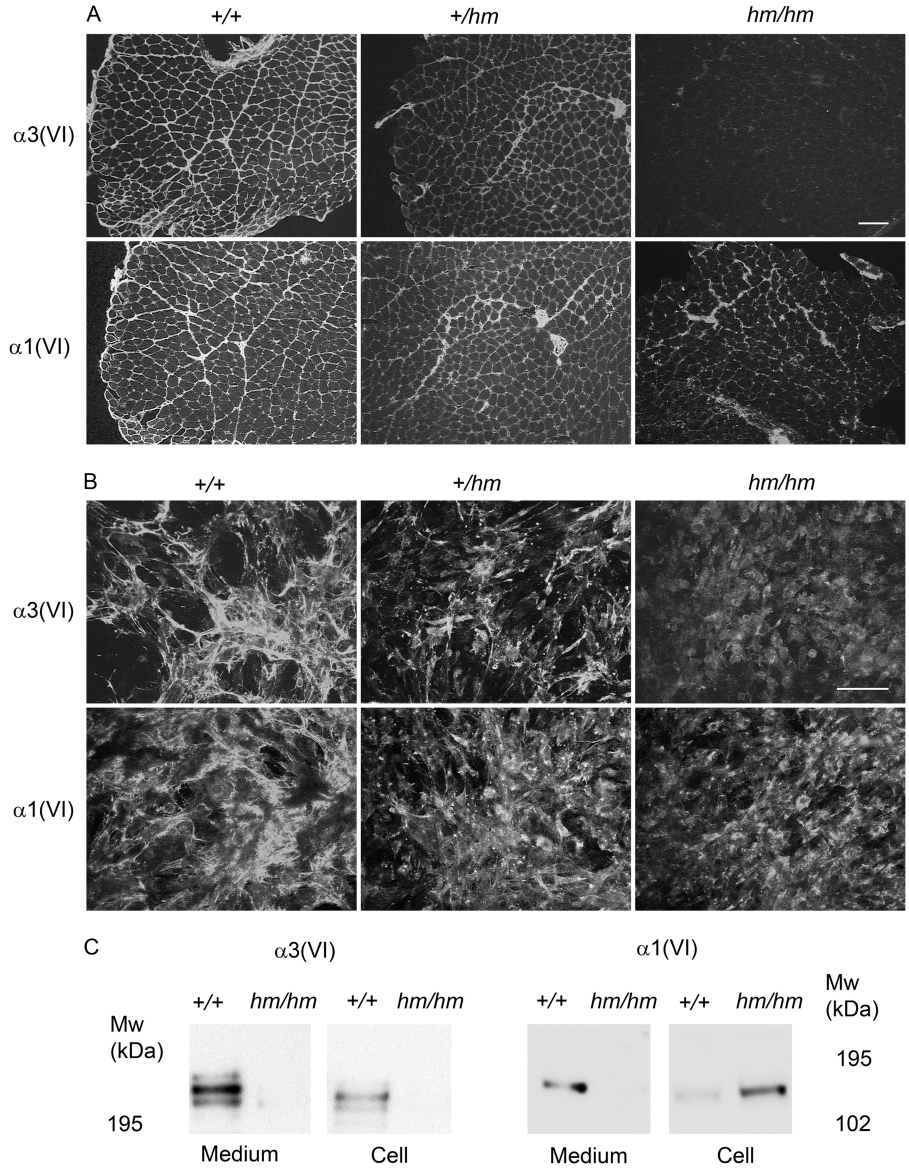

FIGURE 2. **Collagen VI deficiency in skeletal muscle and dermal fibroblasts of the *Col6a3* mutant mice.** *A*, cryosections of quadriceps muscles from 1-month-old *Col6a3*$^{+/+}$, *Col6a3*$^{+/hm}$, and *Col6a3*$^{hm/hm}$ littermates immunostained with polyclonal antibodies specific for the α3(VI) and α1(VI) collagens. *B*, immunostaining of collagen VI deposited by fibroblasts from the *Col6a3*$^{+/+}$, *Col6a3*$^{+/hm}$, and *Col6a3*$^{hm/hm}$ littermates. Cells were grown in the presence of 50 μg/ml ascorbate phosphate for 4 days postconfluence and then stained with polyclonal antibodies specific for the α3(VI) and α1(VI) collagens. Note the intracellular accumulation of the α1(VI) collagen in the *Col6a3*$^{+/hm}$ and *Col6a3*$^{hm/hm}$ fibroblasts. *Magnification bars*, 50 μm. *C*, Western blot analysis of culture medium and cell extracts from dermal fibroblasts of *Col6a3*$^{hm/hm}$ and *Col6a3*$^{+/+}$ mice using antibodies specific for the α3(VI) collagen (*left panels*) and α1(VI) collagen (*right panels*). Very low levels of the α3(VI) collagen were found in both culture medium and cell extracts of the *Col6a3*$^{hm/hm}$ fibroblasts. The α1(VI) collagen was barely detectable in the culture medium the *Col6a3*$^{hm/hm}$ fibroblasts, but its amount was significantly higher in the cell extract of the *Col6a3*$^{hm/hm}$ fibroblasts than in the *Col6a3*$^{+/+}$ counterpart.

to the deletion of exons 15 and 16 (Fig. 1*E*). Thus, contrary to our prediction, the gene targeting event generated a hypomorphic mutation in *Col6a3.* The mutant allele is designated *Col6a3*^{hm}. The resultant mutant α3(VI) collagen chain contained an in-frame deletion encompassing a cysteine-rich linker region and the beginning of the triple-helical domain. As the cysteine-rich sequence is critical for stabilizing the triple-helical collagen VI molecule, its deletion would prevent the mutant chain from assembling into a stable collagen VI triple-helical monomer.

Deficiency of Collagen VI in Col6a3$^{hm/hm}$ *Mice*—Collagen VI expression was examined in the wild type (*Col6a3*$^{+/+}$), heterozygous (*Col6a3*$^{+/hm}$), and homozygous (*Col6a3*$^{hm/hm}$) littermates. Immunostaining of gastrocnemius muscles with the α3(VI) collagen-specific antibody revealed that this chain was barely detectable in *Col6a3*$^{hm/hm}$ and was substantially reduced in *Col6a3*$^{+/hm}$ (Fig. 2*A*). The α1(VI) collagen expression was similarly reduced in the *Col6a3*$^{+/hm}$ muscle, but a low level could be detected in the *Col6a3*$^{hm/hm}$ muscle (Fig. 2*A*). Dermal fibroblasts were established from littermates of all three genotypes and analyzed for the deposition of collagen VI microfibrils. Immunostaining with the α3(VI) collagen-specific antibody showed that extracellular collagen VI microfibrils were abundant in the wild type fibroblasts, significantly reduced in *Col6a3*$^{+/hm}$, and barely detectable in the *Col6a3*$^{hm/hm}$ cells (Fig. 2*B*). The decreases in extracellular col-

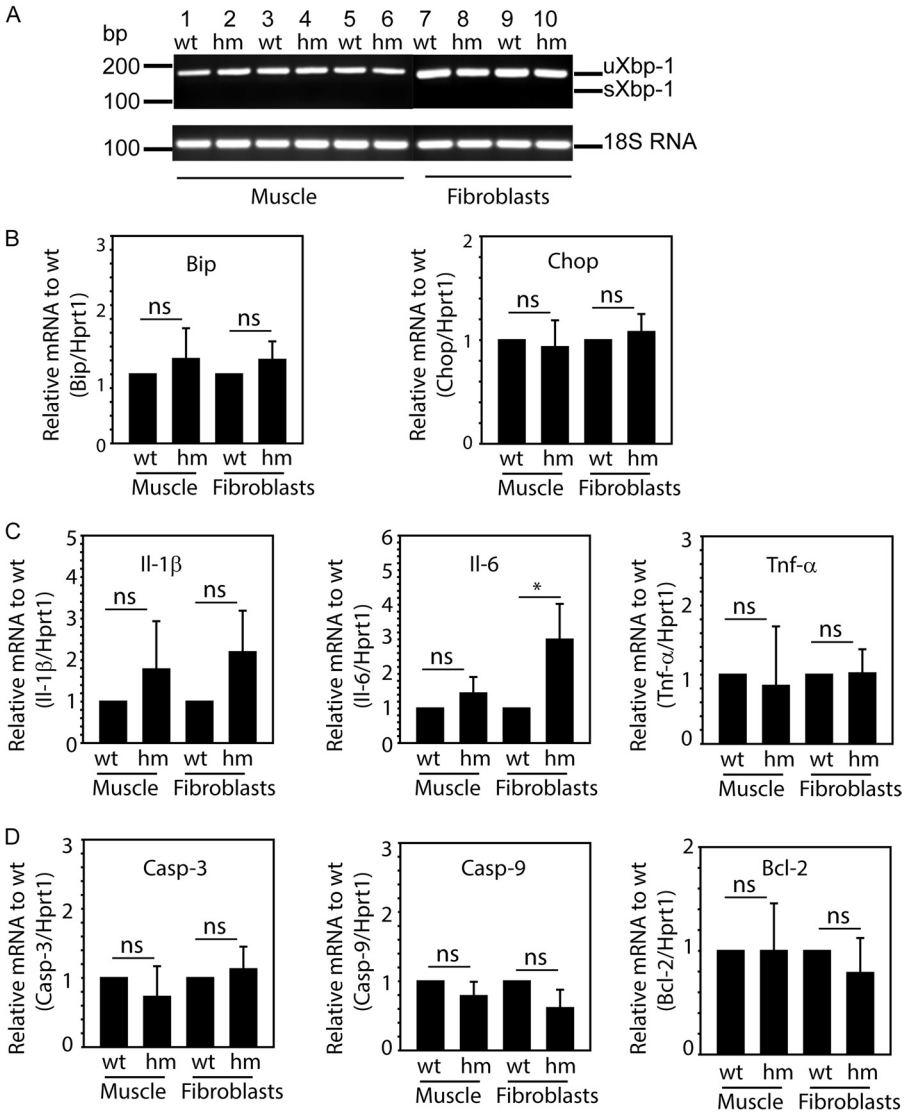

FIGURE 3. **RT-PCR analysis of markers for ER stress, inflammation, and apoptosis in *Col6a3*$^{hm/hm}$ and *Col6a3*$^{+/+}$ mice.** *A*, RT-PCR analysis of total RNA from quadriceps muscles of *Col6a3*$^{+/+}$ (*wt*) and *Col6a3*$^{hm/hm}$ (*hm*) mice at ages 5 days (*lanes 1* and *2*), 1 month (*lanes 3* and *4*), and 3 months (*lanes 5* and *6*) and total RNA from dermal fibroblasts of two separate litters of *Col6a3*$^{+/+}$ (*wt*) and *Col6a3*$^{hm/hm}$ (*hm*) mice. PCR products were run on a 2% agarose gel. Unspliced *Xbp-1* mRNA (*uXbp-1*; 170 bp) was detected in all samples. Spliced *Xbp-1* mRNA (*sXbp-1*; 144 bp), which is induced during ER stress, was absent. *B*, *C*, and *D*, real time RT-PCR analysis of ER stress markers *Bip* and *Chop*; inflammation markers *Il-1β*, *Il-6*, and *Tnf-α*, and apoptosis markers *Casp-3*, *Casp-9*, and *Bcl-2*. Muscle analyses include total RNA isolated from quadriceps muscles of 5-day-, 1-month-, and 3-month-old *Col6a3*$^{+/+}$ (*wt*) and *Col6a3*$^{hm/hm}$ (*hm*) mice. Fibroblast analyses include total RNA prepared from dermal fibroblasts of three pairs of newborn *Col6a3*$^{+/+}$ (*wt*) and *Col6a3*$^{hm/hm}$ (*hm*) littermates. PCRs were done in duplicate for each RNA samples, and mRNA expression of each gene was normalized to that of the *Hprt1* gene. Values of the *Col6a3*$^{hm/hm}$ (*hm*) are expressed as -fold over *Col6a3*$^{+/+}$ (*wt*) and mean ± S.D. (*error bars*). *, $p < 0.05$ between *Col6a3*$^{hm/hm}$ and *Col6a3*$^{+/+}$; *ns*, not significant.

lagen VI microfibrils were similarly observed when the α1(VI) collagen-specific antibody was used except that substantial intracellular reactivity was found in the *Col6a3*$^{+/hm}$ and *Col6a3*$^{hm/hm}$ fibroblasts. Western blot detected much lower levels of the α3(VI) collagen in the culture medium and cell extract of dermal fibroblasts from the *Col6a3*$^{hm/hm}$ mice compared with the wild type counterparts (Fig. 2*C*). The α1(VI) collagen level was also very low in the culture medium of the *Col6a3*$^{hm/hm}$ fibroblasts but was much higher in the cell extract of the *Col6a3*$^{hm/hm}$ fibroblasts compared with the wild type cells. Together, the results demonstrate that the *Col6a3*$^{hm/hm}$ mice are deficient in collagen VI protein in the extracellular matrix and display intracellular retention of the α1(VI) collagen.

To determine whether intracellular accumulation of collagen VI chains in the *Col6a3*$^{hm/hm}$ mice would induce ER stress and the unfolded protein response, the expression of selected molecular markers for the ER stress pathway (26) was examined using RNA isolated from quadriceps muscles and dermal fibroblasts. By RT-PCR, splicing of X-box-binding protein 1 (*Xbp-1*) mRNA induced by ER stress was not detected in skeletal muscles and dermal fibroblasts of *Col6a3*$^{hm/hm}$ mice (Fig. 3*A*). Quantitative RT-PCR analysis did not show a significant difference between the *Col6a3*$^{hm/hm}$ and *Col6a3*$^{+/+}$ mice in the expression of mRNAs for two additional ER stress markers, chaperone-binding protein (*Bip*) and CCAAT/enhancer-binding protein homologous protein (*Chop*) (Fig. 3*B*). In addition, no significant difference was found in mRNA expression of

TABLE 2
Morphometric properties of the *Col6a3* mutant mice
Male mice were used. Results are presented as mean ± S.E.M.

Weight	*+/+*	*hm/hm*
	n=10	**n=9**
Body (g)	21.8±2.3	19.4±3.8
Organ (mg)		
Heart	124.7.6±19.0	115.6±22.3
Liver	723.6±113.8	584.1±226.0
Muscle (mg)	**n= 14 muscles**	**n= 14 muscles**
EDL	11.4±1.5	10.1±1.2**
Soleus	7.5±1.7	5.8±1.6**
Gastrocnemius	120.8±37.8	103.7±19.2
Tibialis Anterior	40.8±6.8	32.5±6.5**
Quadriceps	153.7±40.2	133.3±26.0
Diaphragm	64.1±15.0 (n=10)	51.3±13.8 (n=10)

** Statistically significant between wild type and mutant ($p < 0.05$).

molecular markers of inflammation (*Il-1β*, *Il-6*, and *Tnf-α*) and apoptosis (*Casp-3*, *Casp-9*, and *Bcl-2*) between the *Col6a3*$^{hm/hm}$ and *Col6a3*$^{+/+}$ mice (Fig. 3, *C* and *D*).

Myopathy and Compromised Muscle Function in Col6a3$^{hm/hm}$ *Mice*—Analysis of adult mice at 4 months of age showed that the body and organ weights of the *Col6a3*$^{hm/hm}$ mice were somewhat reduced compared with the *Col6a3*$^{+/+}$ controls, although a statistical significance was not reached (Table 2). Weights of EDL, soleus, and tibialis anterior muscles in the mutant mice were significantly lower than the corresponding muscles from the wild type controls ($p < 0.05$). Gastrocnemius, quadriceps, and diaphragm muscles in the mutant mice also showed decreases in weight, but statistical significance was not reached. The difference in the body weight between the *Col6a3*$^{hm/hm}$ mice and wild type mice was more pronounced with age. The body weights of 1.5–2.0-year-old *Col6a3*$^{hm/hm}$ and their wild type littermates were 23.9 ± 3.9 and 32 ± 2.4 g, respectively ($n = 4$ for each group; $p < 0.05$). No gross skeletal abnormalities were seen in aged mutant mice.

Mild myopathic symptoms could be detected by histology. A wide variation in fiber sizes with many small sized fibers and an increase in the interstitial connective tissue between muscle fibers were observed in gastrocnemius, quadriceps, and diaphragm muscles of the *Col6a3*$^{hm/hm}$ mice compared with the *Col6a3*$^{+/+}$ controls (Fig. 4*A*). Also evident was the presence of regenerative fibers in the *Col6a3*$^{hm/hm}$ mice, indicated by centrally localized nuclei, in contrast to the wild type controls (Fig. 4*A*). The percentage of the central nucleation and distribution of single fiber areas in gastrocnemius muscle sections of the two genotypes were quantified (Fig. 4, *B* and *C*). The gastrocnemius muscle of 6-month-old *Col6a3*$^{hm/hm}$ mice showed increased immunoreactivity with an antibody against collagen type I (Fig. 4, *D* and *E*), suggesting accelerated collagen I deposition and fibrosis progression.

To evaluate muscle function, physiological measurements were performed using dissected EDL muscles. The analyses showed that the EDL muscles from mutant mice were weaker than those of the wild type controls. Absolute and specific forces of both twitch and tetanic contractions were significantly reduced in *Col6a3*$^{hm/hm}$ compared with the wild type mice (Table 3). The decline in absolute force was more pronounced compared with the change in specific force, reflecting the fact that the EDL in *Col6a3*$^{hm/hm}$ was smaller. Notably, there was little difference in ECC force drop generated by the first and fifth tetani under eccentric conditions in *Col6a3*$^{hm/hm}$ when compared with the wild type animals.

Expression of Matrix Proteins in Col6a3 Mutant Muscle—To determine whether there are changes in the expression of selected extracellular matrix proteins and receptors that are known to or likely interact with collagen VI, quadriceps muscles from *Col6a3*$^{+/+}$, *Col6a3*$^{+/hm}$, and *Col6a3*$^{hm/hm}$ littermates were analyzed by immunostaining (Fig. 5). Laminin β1 was expressed in the muscle basement membranes and was comparable among the three genotypes. The basement membrane staining pattern demonstrated wide variations in muscle diameters in the *Col6a3*$^{+/hm}$ and *Col6a3*$^{hm/hm}$ mice compared with the wild type animal. The expression of tenascin-X was increased in the *Col6a3*$^{+/hm}$ and *Col6a3*$^{hm/hm}$ mice compared with the wild type mice (total fluorescence measurements of four non-overlapping images were 2.3 ± 0.5-fold in *Col6a3*$^{hm/hm}$ and 1.9 ± 0.6-fold in *Col6a3*$^{+/hm}$ *versus* *Col6a3*$^{+/+}$). However, there was no significant difference among the three genotypes in the expression of other matrix proteins and receptors examined, including perlecan, decorin, biglycan, matrilin-2 and -4, integrin α7B, and NG2 receptor (data not shown).

Abnormal Collagen Fibril Structure in Tendon, but Not Cornea, of the Col6a3$^{hm/hm}$ *Mice*—Collagen VI is a major component of both tendon and cornea; therefore, to determine the role in non-muscle tissues, an analysis of matrix structure was performed using transmission electron microscopy and 1-month-old *Col6a3*$^{hm/hm}$ and *Col6a3*$^{+/+}$ littermates. In flexor digitorum longus tendons of the wild type mice, a mixture of large and small collagen fibrils was seen (Fig. 6*A*, *panels a*, *b*, and *c*). In contrast, the collagen fibrils in the *Col6a3*$^{hm/hm}$ tendons exhibited a substantial increase in the number of small diameter fibrils throughout the tendon (Fig. 6*A*, *panels d*, *e*, and *f*). In addition, aberrant fibrils with highly irregular profiles, including irregular fibril contours, were observed. There was a regional difference in that the number of small diameter fibrils, aberrant fibrils, and abnormally large diameter fibrils were concentrated in the pericellular region close to the tendon cells (Fig. 6*A*, *panel e*) and less abundant in areas distant from the cells (Fig. 6*A*, *panel f*). Contrary to the observations in tendons, the collagen fibril structure in the cornea of 1-month-old *Col6a3*$^{hm/hm}$ was comparable with that of the wild type littermates (Fig. 6*B*).

DISCUSSION

We have generated and characterized a mutant mouse deficient in the normal α3(VI) collagen chain. First, our gene targeting approach yielded a mouse model with significantly reduced expression of the mutant *Col6a3* gene. The gene-targeting vector was designed to cause a translational frameshift in exon 15 of the *Col6a3* gene and thereby prevent the synthesis of the α3(VI) collagen chain. However, the insertion of the *Pgk-Neo* gene in a small exon of 93 bp inactivated the 5′ splice acceptor site of exon 15, resulting in splicing from exon 14 to exon 17 (Fig. 1*E*). Analysis of the heterozygous mutant mouse indicates a substantial reduction in the expression of the mutant allele compared with the wild type counterpart (Fig. 1*D*). The reduced expression observed is consistent with previ-

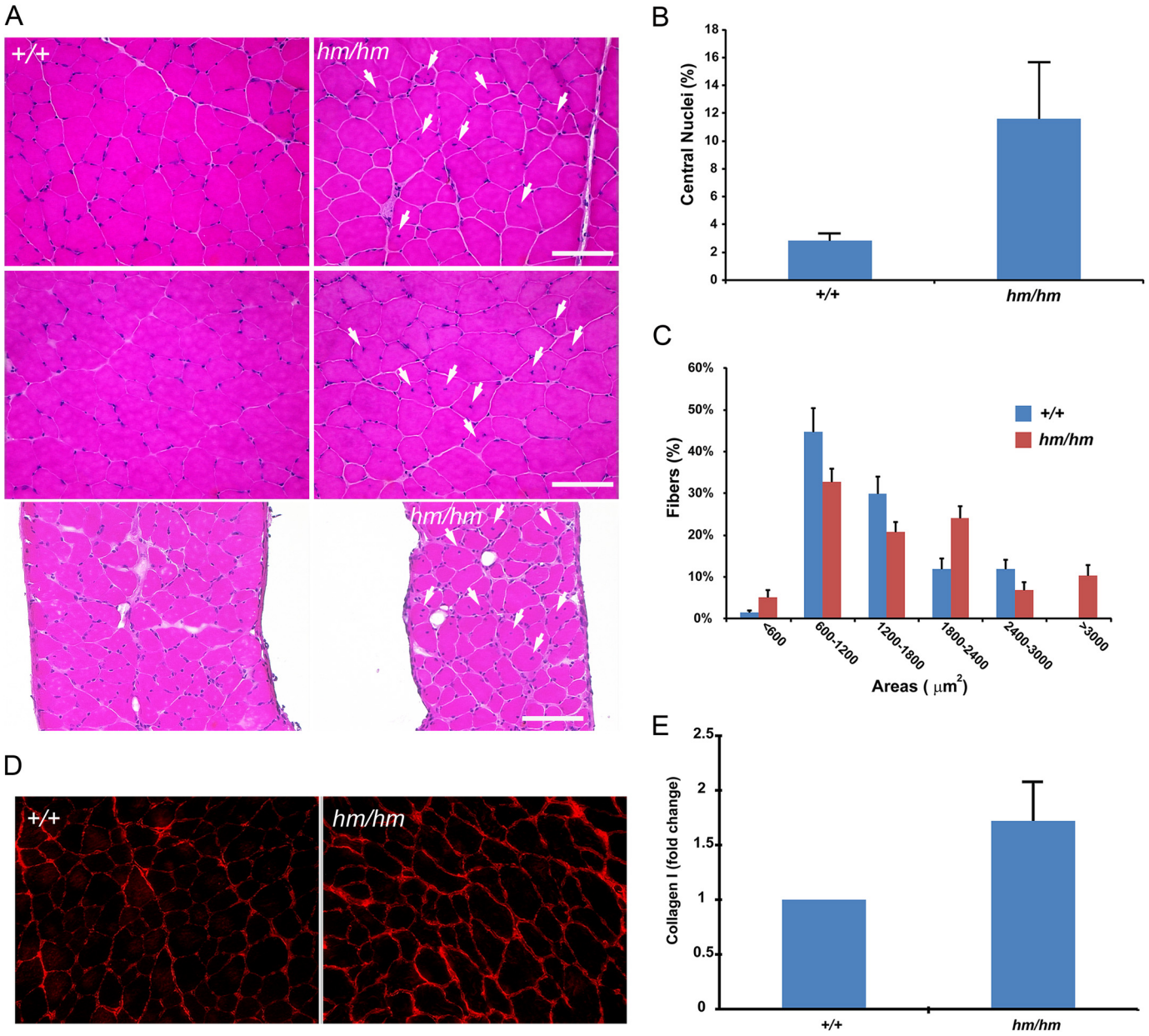

FIGURE 4. **Analysis of limb and diaphragm muscles of the *Col6a3* mouse mutant.** *A*, cryosections of gastrocnemius (*Gas*), quadriceps (*Qua*), and diaphragm (*Dia*) muscles of *Col6a3*$^{+/+}$ and *Col6a3*$^{hm/hm}$ mice were stained with hematoxylin and eosin. Centrally localized nuclei (*arrows*) are abundant in the *Col6a3*$^{hm/hm}$ muscles but barely detectable in the *Col6a3*$^{+/+}$ controls. An increase in the interstitial connective tissue between muscle fibers is evident in the *Col6a3*$^{hm/hm}$ mice compared with the *Col6a3*$^{+/+}$ control. *Magnification bars*, 50 μm. *B*, quantification of the percentage of gastrocnemius muscles with centrally located nuclei in *Col6a3*$^{+/+}$ and *Col6a3*$^{hm/hm}$ mice. *C*, distribution of single fiber areas in gastrocnemius muscles from *Col6a3*$^{+/+}$ and *Col6a3*$^{hm/hm}$ mice. The *Col6a3*$^{hm/hm}$ muscles show a wide variation in fiber size compared with the *Col6a3*$^{+/+}$ control. Data in *B* and *C* were from four muscles per group and are expressed as mean ± S.E. (*error bars*). *D*, increased immunoreactivity of type I collagen in *Col6a3*$^{hm/hm}$ muscle. Cryosections of quadriceps muscles from 6-month-old *Col6a3*$^{+/+}$ and *Col6a3*$^{hm/hm}$ mice were immunostained with affinity-purified antibody against type I collagen. A representative image is shown. *E*, quantification of increased immunoreactivity with type I collagen in *Col6a3*$^{hm/hm}$ quadriceps muscles. The percent area positive for type I collagen in four muscles per group was analyzed using ImageJ software. Values are expressed as -fold change over *Col6a3*$^{+/+}$ and as mean ± S.E. (*error bars*).

ous findings that insertion of a selectable marker in a gene suppresses its expression (27, 28). Second, in the mutant allele, skipping of exons 15 and 16 results in an in-frame deletion of 49 amino acids in the mutant α3(VI) collagen chain. The mutant α3(VI) collagen chain likely can be assembled into a triple-helical collagen VI molecule as biochemical and genetic evidence suggests that collagen VI chain assembly proceeds in the direction of C to N terminus (29, 30). However, the assembled triple-helical collagen VI molecule would be unstable because the mutant α3(VI) collagen chain lacks the cysteine-rich linker segment that stabilizes the triple-helical monomer. This prevents the formation of collagen VI microfibrils extracellularly. Thus, the *Col6a3*^{hm} allele should be equivalent to a functional null allele. This interpretation is supported by the observation that *Col6a3*$^{hm/hm}$ fibroblasts assemble few collagen VI microfibrils, and the *Col6a3*$^{+/hm}$ cells deposit approximately half the amount of collagen VI microfibrils compared with the wild type fibroblasts (Fig. 2*B*).

Intracellular accumulation of the α1(VI) collagen chain was found in dermal fibroblasts from both *Col6a3*$^{+/hm}$ and

Col6a3$^{hm/hm}$ mice (Fig. 2*B*). This indicates that synthesis of the individual collagen VI chain is independently regulated. In the absence of a functional α3(VI) collagen chain, the excess α1(VI) chain is accumulated in the cytoplasm, which also may contribute to the abnormal phenotype. However, the molecular markers of the ER stress pathway were not increased in the *Col6a3*$^{hm/hm}$ muscles and dermal fibroblasts (Fig. 3, *A* and *B*). Our result is consistent with the finding in patients with collagen VI mutations that intracellular retention of collagen VI α chains does not increase ER stress markers (31).

Analysis of the *Col6a3*$^{hm/hm}$ mouse mutant demonstrates that a deficiency in the normal α3(VI) collagen chain results in a relatively mild gross and muscle phenotype similar to that of the previously reported *Col6a1*-null mice (32). Both mouse models have normal life spans unlike patients with severe deficiency of collagen VI who have a high risk of early death. Similar to the *Col6a1*-null mice, the *Col6a3*$^{hm/hm}$ mice exhibit mild myopathic pathology and compromised muscle contractile forces (Fig. 4 and Table 3) (32, 33). Although the *Col6a1*-null muscles show spontaneous apoptosis (33), the *Col6a3*$^{hm/hm}$ muscles do not exhibit a significant increase in the expression of molecular makers for apoptosis compared with wild type controls (Fig. 3*D*). It should be noted that mice from ages 5 days to 3 months were used in our analysis to mimic the childhood onset of collagen VI muscular dystrophy. The lack of a significant increase in markers for apoptosis in the *Col6a3*$^{hm/hm}$ mice could be because the degree of apoptosis in young animals is usually low. The *Col6a3*$^{hm/hm}$ muscles do not display significantly increased inflammation (Fig. 3*C*), and they show a slight increase in fibrosis (Fig. 3, *D* and *E*). This is likely due to the mild myopathic phenotype of mice deficient in collagen VI. Whether the *Col6a3*$^{hm/hm}$ muscles display mitochondrial dysfunction and defective autophagy as demonstrated in the *Col6a1*-null mice (33, 34) awaits a comprehensive analysis of the *Col6a3*$^{hm/hm}$ mice in the future.

TABLE 3

Contractile properties of the EDL muscle in *Col6a3* mutant mice

Male mice were used. Results are presented as mean ± S.E.M. CSA, cross-sectional area; Lo, optimal length; mN, millinewtons.

	+/+ ($n = 14$ muscles)	*hm/hm* ($n = 14$ muscles)
Twitch		
Absolute force (mN)	70.4 ± 20.5	47.6 ± 20.4[a]
Specific force (mN/mm^2)	32.1 ± 9.9	22.6 ± 10.5[a]
Specific force (mN/mg)	6.3 ± 2.0	4.7 ± 1.2[a]
Tetanus		
Absolute force (mN)	312.0 ± 68.2	208.4 ± 43.4[a]
Specific force (mN/mm^2)	143.2 ± 41.1	97.4 ± 43.4[a]
Specific force (mN/mg)	28.4 ± 8.8	20.8 ± 9.0[a]
ECC force drop 1–5 (%)	34.6 ± 18.3	31.5 ± 19.0
EDL Lo (mm)	10.7 ± 0.8	9.9 ± 1.0[a]
CSA (mm^2) by Brooks-Faulkner	2.2 ± 0.3	2.2 ± 0.3

[a] Statistically significant between wild type and mutant ($p < 0.05$).

The marked reduction in collagen VI expression in muscles of the *Col6a3* mutant mice (Fig. 2) suggests that the three α3(VI)-like collagen chains, *i.e.* α4(VI), α5(VI), and α6(VI), are unable to compensate for the loss of normal α3(VI) collagen. This is consistent with the highly restricted tissue distribution patterns of the α3(VI)-like chains (11–13). Specifically, only the α6(VI) chain can be detected in the endomysium and perimysium of the skeletal muscle (13). The low level of α1(VI) chain immunoreactivity seen in the muscle tissue of *Col6a*$^{hm/hm}$ (Fig. 2*A*) could result from microfibrils with α1(VI)α2(VI)α6(VI) chain composition.

Previous studies suggest that the C-terminal C5 domain of the α3(VI) collagen is proteolytically processed after assembling into microfibrils and that the cleaved C5 domain can be found in tumor endothelium where it interacts with tumor endothelial marker 8 (6, 8, 9). Recently, the C-terminal cleavage product produced by the adipose tissue has been shown to pro-

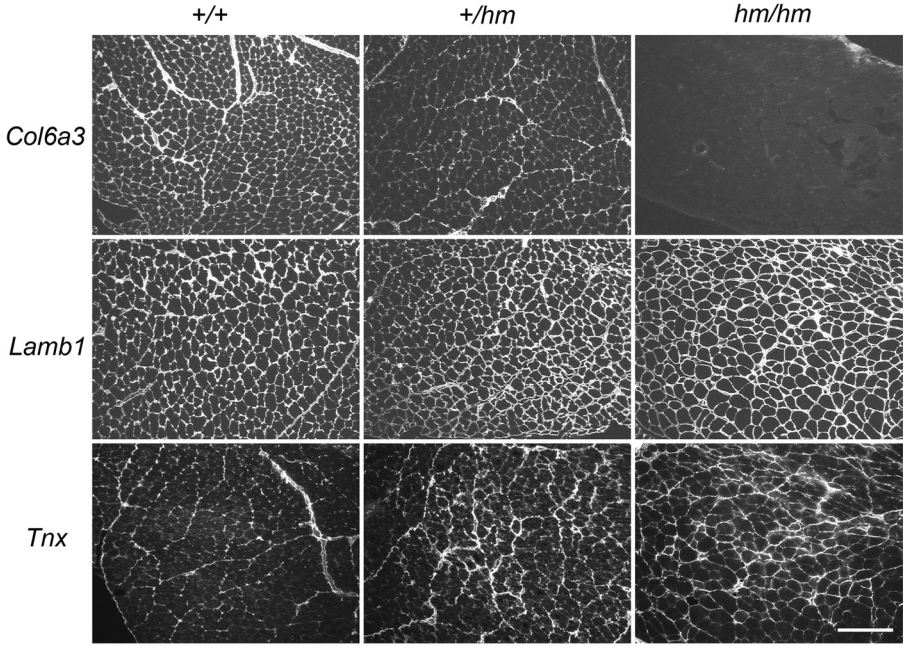

FIGURE 5. **Immunofluorescence staining of skeletal muscles with antibodies for selected extracellular matrix proteins.** Cryosections of quadriceps muscles from 1-month-old *Col6a3*$^{+/+}$, *Col6a3*$^{+/hm}$, and *Col6a3*$^{hm/hm}$ mice were stained with polyclonal antibodies against α3(VI) collagen (*Col6a3*), laminin β1 (*Lamb1*), and tenascin-X (*Tnx*). The expression of tenascin-X was increased in the *Col6a3*$^{+/hm}$ and *Col6a3*$^{hm/hm}$ mice. *Magnification bar*, 100 μm.

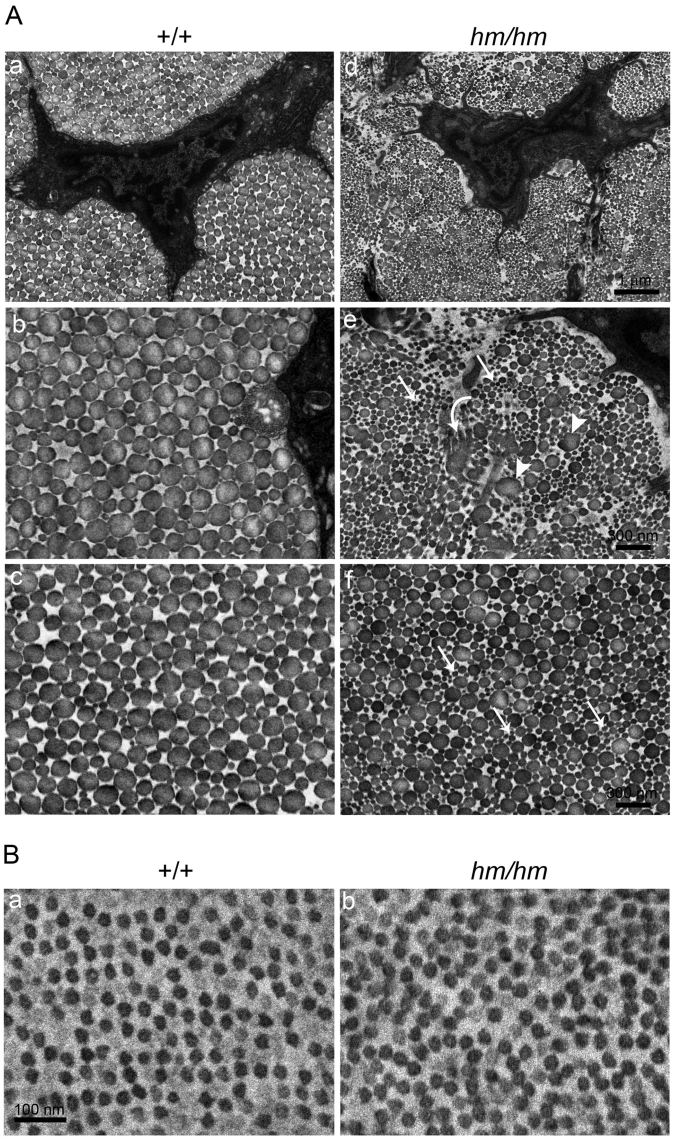

FIGURE 6. **Abnormal collagen fibril assembly in tendon, but not cornea, of the *Col6a3*$^{hm/hm}$ mice.** Transmission electron micrographs of tendons and corneas from 1 month-old *Col6a3*$^{+/+}$ and *Col6a3*$^{hm/hm}$ mice are shown. *A*, flexor digitorum longus tendons. Low magnification images (*panels a* and *d*; *scale bar*, 1 μm) show disorganization of cell and matrix in the *Col6a3*$^{hm/hm}$ tendon (*panel d*) compared with the *Col6a3*$^{+/+}$ tendon (*panel a*). At high magnification, collagen fibrils from the *Col6a3*$^{+/+}$ mice (*panels b* and *c*) display normal cross-sectional profiles in both central (*panel c*) and pericellular (*panel b*) regions. The fibrils are circular with a heterogeneous distribution of fibril diameters. In contrast, the *Col6a3*$^{hm/hm}$ tendons (*panels e* and *f*) have larger numbers of smaller diameter fibrils (*arrows*) in both central (*panel f*) and pericellular (*panel e*) areas. Very large, twisted, and structurally abnormal fibrils (*arrowheads* and *curved arrow*) are found in the pericellular (*panel e*), but not central (*panel f*), areas. *Scale bars*, 100 nm. *B*, cornea. Collagen fibrils in corneal stroma of *Col6a3*$^{+/+}$ (*panel a*) and *Col6a3*$^{hm/hm}$ (*panel b*) are comparable. *Scale bar*, 100 nm.

mote cancer progression in mouse models of breast cancer (10). The lack of a severe phenotype in the α3(VI) collagen mutant mouse implies that the large N- and C-globular domains of the α3(VI) α chain do not serve indispensable functions independent of collagen VI microfibril assembly during normal growth and development. Whether the marked reduction of the C5 domain affects tumor formation or progression in the homozygous mouse remains to be investigated.

Physiological measurements of muscle function demonstrate that there are significant differences in both absolute and specific force generated by a single twitch or tetanic stimulation (Table 3). This is consistent with the muscle weakness in mutant animals. In both twitch and tetanic stimulation, the force decrease was more remarkable and significant for the absolute force, whereas the drop in specific force was less pronounced. This difference is explained by the reduced EDL muscle weight noted in the mutant animals (Table 2) so that the decrease in specific force is amplified when calculated for the whole muscle. Interestingly, we did not record any significant drop in ECC comparing the first and fifth eccentric tetanic contractions in the *Col6a3* mouse mutant (Table 3). ECC force drop is a physiological hallmark of the *mdx* mouse model of Duchenne muscular dystrophy due to a deficiency in dystrophin (35, 36). This is thought to be due to the inherent instability of the plasma membrane and lack of costameric stability resulting from the lack of dystrophin in the *mdx* mouse model and in patients with Duchenne muscular dystrophy, leading to active degeneration and regeneration in the muscle. Severe collagen VI deficiency causing the clinical phenotype of Ullrich congenital muscular dystrophy is a much less dystrophic myopathy at least early in the disease course (37), indicating that mechanical fragility of the plasma membrane is not as important in this muscle disease compared with the conditions caused by deficiencies of dystrophin or of the dystrophin-associated glycoprotein complex. In keeping with this hypothesis is that serum creatine kinase levels in patients with collagen VI deficiency are frequently normal or only mildly elevated. Thus, the mechanisms leading to muscle disease in collagen VI deficiency are different from those of the classic muscular dystrophies.

Although a decrease in laminin β1 expression was previously found in patients with collagen VI congenital muscular dystrophy (38), we found no difference in laminin β1 reactivity in collagen VI-deficient mice compared with the wild type controls (Fig. 5). Our results show that tenascin-X protein expression is increased in muscle deficient in collagen VI (Fig. 5). In humans, the absence of tenascin-X leads to a recessive form of Ehlers-Danlos syndrome characterized by joint hypermobility and skin hyperextensibility (39). The connective tissue abnormalities partially overlap with those of collagen VI muscular dystrophy (40, 41). Additionally, a mild myopathic phenotype has been described recently in mice lacking tenascin-X (42). These findings suggest that there may be a functional overlap between collagen VI and tenascin-X so that there is a compensatory increase in tenascin-X in the endomysium of collagen VI-deficient muscle. To this end, both collagen VI and tenascin-X are able to modulate collagen I fibrillogenesis *in vitro*, and deficiency in either protein leads to abnormal collagen fibrils (43, 44). On the other hand, contrary to expectation based on the compensatory hypothesis, collagen VI mRNA and protein expression is decreased in fibroblasts from tenascin-X-null mice (43).

Our ultrastructural analysis of the *Col6a3*$^{hm/hm}$ tendon is consistent with the finding in *Col6a1*-null mice indicating an association between deficiency in collagen VI and abnormal tendon collagen fibril assembly/structure (25). Collagen VI is a

key component in the pericellular matrix of tendons and ligaments (45). Our studies demonstrate that the absence of collagen VI alters organization of the tendon fibroblasts and the pericellular collagen fibril-forming microdomains defined by the fibroblast surface. The precise molecular mechanisms by which collagen VI modulates collagen I fibril assembly are not known but are likely to be indirect, mediated through changes in the expression of molecules that regulate collagen fibrillogenesis by tendon fibroblasts. For instance, a consistent small increase in MMP-2 activity has been found in the *Col6a1*-null tendon (25). In addition, collagen VI binds a number of extracellular molecules such as small leucine-rich repeat proteoglycans and fibril-associated collagens with interrupted triple helices that have been implicated in regulation of the later stages in fibril assembly (46). It is possible that lack of collagen VI provides additional interactions with the collagen fibrils, thus altering fibril structure in the mature tendon. This would be consistent with the maintenance of small diameter fibrils observed in the mutant tendons. Collagen VI is also a major component of cornea and is closely associated with cornea fibroblasts (47). However, we found that collagen fibrillogenesis in the cornea is not affected by the absence of collagen VI. Collagen fibrils in the cornea are homogenously small diameter as they do not undergo lateral growth during fibril maturation unlike collagen fibrils in most other connective tissues (48). In addition, higher concentrations of the regulatory molecules are found in the corneal stroma compared with the tendon so that the absence of interactions with collagen VI would not be as significant as in the tendon. Our demonstration of a tendinopathy in the *Col6a3*$^{hm/hm}$ mouse has direct implications for the human collagen VI-related myopathies as the joint hyperlaxity and more importantly the striking progressive joint contractures are a significant contributor to the morbidity and disease progression. Because the contractures typically are out of proportion to the muscle weakness, the tendon abnormalities identified in our mouse model likely contribute significantly to the disease in patients.

In conclusion, our studies demonstrated that mice lacking a functional α3(VI) collagen α chain display muscle and tendon features reminiscent of human patients albeit with significantly milder phenotypic manifestation. Thus, the mouse mutant represents a second model for recessive collagen VI muscular dystrophy and can be utilized to further understand the consequence of *COL6A3* dysfunction.

Acknowledgments—We thank Drs. Larry Fisher, Ken-Ichi Matsumoto, William Stallcup, Ulrike Mayer, and Mats Paulsson for providing antibodies.

REFERENCES

1. Chu, M. L., Conway, D., Pan, T. C., Baldwin, C., Mann, K., Deutzmann, R., and Timpl, R. (1988) Amino acid sequence of the triple-helical domain of human collagen type VI. *J. Biol. Chem.* **263,** 18601–18606
2. Chu, M. L., Pan, T. C., Conway, D., Kuo, H. J., Glanville, R. W., Timpl, R., Mann, K., and Deutzmann, R. (1989) Sequence analysis of α1(VI) and α2(VI) chains of human type VI collagen reveals internal triplication of globular domains similar to the A domains of von Willebrand factor and two α2(VI) chain variants that differ in the carboxy terminus. *EMBO J.* **8,** 1939–1946
3. Chu, M. L., Zhang, R. Z., Pan, T. C., Stokes, D., Conway, D., Kuo, H. J., Glanville, R., Mayer, U., Mann, K., and Deutzmann, R. (1990) Mosaic structure of globular domains in the human type VI collagen α3 chain: similarity to von Willebrand factor, fibronectin, actin, salivary proteins and aprotinin type protease inhibitors. *EMBO J.* **9,** 385–393
4. Zanussi, S., Doliana, R., Segat, D., Bonaldo, P., and Colombatti, A. (1992) The human type VI collagen gene. mRNA and protein variants of the α3 chain generated by alternative splicing of an additional 5-end exon. *J. Biol. Chem.* **267,** 24082–24089
5. Furthmayr, H., Wiedemann, H., Timpl, R., Odermatt, E., and Engel, J. (1983) Electron-microscopical approach to a structural model of intima collagen. *Biochem. J.* **211,** 303–311
6. Aigner, T., Hambach, L., Söder, S., Schlötzer-Schrehardt, U., and Pöschl, E. (2002) The C5 domain of Col6A3 is cleaved off from the Col6 fibrils immediately after secretion. *Biochem. Biophys. Res. Commun.* **290,** 743–748
7. Lamandé, S. R., Mörgelin, M., Adams, N. E., Selan, C., and Allen, J. M. (2006) The C5 domain of the collagen VI α3(VI) chain is critical for extracellular microfibril formation and is present in the extracellular matrix of cultured cells. *J. Biol. Chem.* **281,** 16607–16614
8. Mayer, U., Pöschl, E., Nischt, R., Specks, U., Pan, T. C., Chu, M. L., and Timpl, R. (1994) Recombinant expression and properties of the Kunitz-type protease-inhibitor module from human type VI collagen α3(VI) chain. *Eur. J. Biochem.* **225,** 573–580
9. Nanda, A., Carson-Walter, E. B., Seaman, S., Barber, T. D., Stampfl, J., Singh, S., Vogelstein, B., Kinzler, K. W., and St Croix, B. (2004) TEM8 interacts with the cleaved C5 domain of collagen α3(VI). *Cancer Res.* **64,** 817–820
10. Park, J., and Scherer, P. E. (2012) Adipocyte-derived endotrophin promotes malignant tumor progression. *J. Clin. Investig.* **122,** 4243–4256
11. Fitzgerald, J., Rich, C., Zhou, F. H., and Hansen, U. (2008) Three novel collagen VI chains, α4(VI), α5(VI), and α6(VI). *J. Biol. Chem.* **283,** 20170–20180
12. Gara, S. K., Grumati, P., Urciuolo, A., Bonaldo, P., Kobbe, B., Koch, M., Paulsson, M., and Wagener, R. (2008) Three novel collagen VI chains with high homology to the α3 chain. *J. Biol. Chem.* **283,** 10658–10670
13. Gara, S. K., Grumati, P., Squarzoni, S., Sabatelli, P., Urciuolo, A., Bonaldo, P., Paulsson, M., and Wagener, R. (2011) Differential and restricted expression of novel collagen VI chains in mouse. *Matrix Biol.* **30,** 248–257
14. Allamand, V., Briñas, L., Richard, P., Stojkovic, T., Quijano-Roy, S., and Bonne, G. (2011) ColVI myopathies: where do we stand, where do we go? *Skelet. Muscle* **1,** 30
15. Bönnemann, C. G. (2011) The collagen VI-related myopathies: muscle meets its matrix. *Nat. Rev. Neurol.* **7,** 379–390
16. Jöbsis, G. J., Boers, J. M., Barth, P. G., and de Visser, M. (1999) Bethlem myopathy: a slowly progressive congenital muscular dystrophy with contractures. *Brain* **122,** 649–655
17. Zhang, R. Z., Pan, T. C., Timpl, R., and Chu, M. L. (1993) Cloning and sequence analysis of cDNAs encoding the α1, α2 and α3 chains of mouse collagen VI. *Biochem. J.* **291,** 787–792
18. Zhang, R. Z., Sabatelli, P., Pan, T. C., Squarzoni, S., Mattioli, E., Bertini, E., Pepe, G., and Chu, M. L. (2002) Effects on collagen VI mRNA stability and microfibrillar assembly of three COL6A2 mutations in two families with Ullrich congenital muscular dystrophy. *J. Biol. Chem.* **277,** 43557–43564
19. Specks, U., Mayer, U., Nischt, R., Spissinger, T., Mann, K., Timpl, R., Engel, J., and Chu, M. L. (1992) Structure of recombinant N-terminal globule of type VI collagen α3 chain and its binding to heparin and hyaluronan. *EMBO J.* **11,** 4281–4290
20. Tillet, E., Wiedemann, H., Golbik, R., Pan, T. C., Zhang, R. Z., Mann, K., Chu, M. L., and Timpl, R. (1994) Recombinant expression and structural and binding properties of α1(VI) and α2(VI) chains of human collagen type VI. *Eur. J. Biochem.* **221,** 177–185
21. Bogdanovich, S., Krag, T. O., Barton, E. R., Morris, L. D., Whittemore, L. A., Ahima, R. S., and Khurana, T. S. (2002) Functional improvement of dystrophic muscle by myostatin blockade. *Nature* **420,** 418–421
22. Bogdanovich, S., McNally, E. M., and Khurana, T. S. (2008) Myostatin blockade improves function but not histopathology in a murine model of

limb-girdle muscular dystrophy 2C. *Muscle Nerve* **37,** 308–316
23. Brooks, S. V., and Faulkner, J. A. (1990) Contraction-induced injury: recovery of skeletal muscles in young and old mice. *Am. J. Physiol. Cell Physiol.* **258,** C436–C442
24. Chen, S., Oldberg, A., Chakravarti, S., and Birk, D. E. (2010) Fibromodulin regulates collagen fibrillogenesis during peripheral corneal development. *Dev. Dyn.* **239,** 844–854
25. Izu, Y., Ansorge, H. L., Zhang, G., Soslowsky, L. J., Bonaldo, P., Chu, M. L., and Birk, D. E. (2011) Dysfunctional tendon collagen fibrillogenesis in collagen VI null mice. *Matrix Biol.* **30,** 53–61
26. Deldicque, L., Hespel, P., and Francaux, M. (2012) Endoplasmic reticulum stress in skeletal muscle: origin and metabolic consequences. *Exerc. Sport Sci. Rev.* **40,** 43–49
27. Meyers, E. N., Lewandoski, M., and Martin, G. R. (1998) An Fgf8 mutant allelic series generated by Cre- and Flp-mediated recombination. *Nat. Genet.* **18,** 136–141
28. Nagy, A., Moens, C., Ivanyi, E., Pawling, J., Gertsenstein, M., Hadjantonakis, A. K., Pirity, M., and Rossant, J. (1998) Dissecting the role of N-myc in development using a single targeting vector to generate a series of alleles. *Curr. Biol.* **8,** 661–664
29. Lamandé, S. R., Mörgelin, M., Selan, C., Jöbsis, G. J., Baas, F., and Bateman, J. F. (2002) Kinked collagen VI tetramers and reduced microfibril formation as a result of Bethlem myopathy and introduced triple helical glycine mutations. *J. Biol. Chem.* **277,** 1949–1956
30. Pan, T. C., Zhang, R. Z., Sudano, D. G., Marie, S. K., Bönnemann, C. G., and Chu, M. L. (2003) New molecular mechanism for Ullrich congenital muscular dystrophy: a heterozygous in-frame deletion in the COL6A1 gene causes a severe phenotype. *Am. J. Hum. Genet.* **73,** 355–369
31. Allamand, V., Merlini, L., and Bushby, K. (2010) 166th ENMC International Workshop on Collagen type VI-related Myopathies, 22–24 May 2009, Naarden, The Netherlands. *Neuromuscul. Disord.* **20,** 346–354
32. Bonaldo, P., Braghetta, P., Zanetti, M., Piccolo, S., Volpin, D., and Bressan, G. M. (1998) Collagen VI deficiency induces early onset myopathy in the mouse: an animal model for Bethlem myopathy. *Hum. Mol. Genet.* **7,** 2135–2140
33. Irwin, W. A., Bergamin, N., Sabatelli, P., Reggiani, C., Megighian, A., Merlini, L., Braghetta, P., Columbaro, M., Volpin, D., Bressan, G. M., Bernardi, P., and Bonaldo, P. (2003) Mitochondrial dysfunction and apoptosis in myopathic mice with collagen VI deficiency. *Nat. Genet.* **35,** 367–371
34. Grumati, P., Coletto, L., Sabatelli, P., Cescon, M., Angelin, A., Bertaggia, E., Blaauw, B., Urciuolo, A., Tiepolo, T., Merlini, L., Maraldi, N. M., Bernardi, P., Sandri, M., and Bonaldo, P. (2010) Autophagy is defective in collagen VI muscular dystrophies, and its reactivation rescues myofiber degeneration. *Nat. Med.* **16,** 1313–1320
35. Moens, P., Baatsen, P. H., and Maréchal, G. (1993) Increased susceptibility of EDL muscles from mdx mice to damage induced by contractions with stretch. *J. Muscle Res. Cell Motil.* **14,** 446–451
36. Petrof, B. J., Shrager, J. B., Stedman, H. H., Kelly, A. M., and Sweeney, H. L. (1993) Dystrophin protects the sarcolemma from stresses developed during muscle contraction. *Proc. Natl. Acad. Sci. U.S.A.* **90,** 3710–3714
37. Schessl, J., Goemans, N. M., Magold, A. I., Zou, Y., Hu, Y., Kirschner, J., Sciot, R., and Bönnemann, C. G. (2008) Predominant fiber atrophy and fiber type disproportion in early Ullrich disease. *Muscle Nerve* **38,** 1184–1191
38. Merlini, L., Villanova, M., Sabatelli, P., Malandrini, A., and Maraldi, N. M. (1999) Decreased expression of laminin β1 in chromosome 21-linked Bethlem myopathy. *Neuromuscul. Disord.* **9,** 326–329
39. Schalkwijk, J., Zweers, M. C., Steijlen, P. M., Dean, W. B., Taylor, G., van Vlijmen, I. M., van Haren, B., Miller, W. L., and Bristow, J. (2001) A recessive form of the Ehlers-Danlos syndrome caused by tenascin-X deficiency. *N. Engl. J. Med.* **345,** 1167–1175
40. Kirschner, J., Hausser, I., Zou, Y., Schreiber, G., Christen, H. J., Brown, S. C., Anton-Lamprecht, I., Muntoni, F., Hanefeld, F., and Bönnemann, C. G. (2005) Ullrich congenital muscular dystrophy: connective tissue abnormalities in the skin support overlap with Ehlers-Danlos syndromes. *Am. J. Med. Genet. A* **132A,** 296–301
41. Voermans, N. C., Jenniskens, G. J., Hamel, B. C., Schalkwijk, J., Guicheney, P., and van Engelen, B. G. (2007) Ehlers-Danlos syndrome due to tenascin-X deficiency: muscle weakness and contractures support overlap with collagen VI myopathies. *Am. J. Med. Genet. A* **143A,** 2215–2219
42. Voermans, N. C., Verrijp, K., Eshuis, L., Balemans, M. C., Egging, D., Sterrenburg, E., van Rooij, I. A., van der Laak, J. A., Schalkwijk, J., van der Maarel, S. M., Lammens, M., and van Engelen, B. G. (2011) Mild muscular features in tenascin-X knockout mice, a model of Ehlers-Danlos syndrome. *Connect. Tissue Res.* **52,** 422–432
43. Minamitani, T., Ariga, H., and Matsumoto, K. (2004) Deficiency of tenascin-X causes a decrease in the level of expression of type VI collagen. *Exp. Cell Res.* **297,** 49–60
44. Minamitani, T., Ikuta, T., Saito, Y., Takebe, G., Sato, M., Sawa, H., Nishimura, T., Nakamura, F., Takahashi, K., Ariga, H., and Matsumoto, K. (2004) Modulation of collagen fibrillogenesis by tenascin-X and type VI collagen. *Exp. Cell Res.* **298,** 305–315
45. Ritty, T. M., Roth, R., and Heuser, J. E. (2003) Tendon cell array isolation reveals a previously unknown fibrillin-2-containing macromolecular assembly. *Structure* **11,** 1179–1188
46. Birk, D. E., and Bruckner, P. (2011) in *The Extracellular Matrix: an Overview* (Mecham, R. P., ed) pp. 77–115, Springer, New York
47. Zimmermann, D. R., Trüeb, B., Winterhalter, K. H., Witmer, R., and Fischer, R. W. (1986) Type VI collagen is a major component of the human cornea. *FEBS Lett.* **197,** 55–58
48. Zhang, G., Chen, S., Goldoni, S., Calder, B. W., Simpson, H. C., Owens, R. T., McQuillan, D. J., Young, M. F., Iozzo, R. V., and Birk, D. E. (2009) Genetic evidence for the coordinated regulation of collagen fibrillogenesis in the cornea by decorin and biglycan. *J. Biol. Chem.* **284,** 8888–8897